Formation of $Ce_{1-x}Pd_xO_{2-\delta}$ Solid Solution in Combustion-Synthesized Pd/CeO_2 Catalyst: XRD, XPS, and EXAFS Investigation

K. R. Priolkar,[†] Parthasarathi Bera,[‡] P. R. Sarode,[†] M. S. Hegde,*[,‡] S. Emura,[§] R. Kumashiro,[¶] and N. P. Lalla[||]

Department of Physics, Goa University, Goa-403206, India, Solid State and Structural Chemistry Unit, Indian Institute of Science, Bangalore 560012, India, Institute of Scientific and Industrial Research, Osaka University, Mihoga-oka 8-1, Ibaraki, Osaka, 567-0047, Japan, Research Laboratory for Surface Science, Faculty of Science, Okayama University, Tsushima-naka, Okayama 700-8530, Japan, and Inter University Consortium, University Campus, Indore 452017, India

Received September 17, 2001. Revised Manuscript Received February 4, 2002

Pd/CeO_2 (1 at. %) prepared by the solution-combustion method shows a higher catalytic activity for CO oxidation and NO reduction than Pd metal, PdO, and Pd dispersed over CeO_2 by the conventional method. To understand the higher catalytic properties, the structure of 1 at. % Pd/CeO_2 catalyst material has been investigated by X-ray diffraction (XRD), X-ray photoelectron spectroscopy (XPS), and extended X-ray absorption fine structure (EXAFS) spectroscopy. The diffraction lines corresponding to Pd or PdO are not observed in the high-resolution XRD pattern of 1 at. % Pd/CeO_2. The structure of 1 at. % Pd/CeO_2 could be refined for the composition of $Ce_{0.99}Pd_{0.01}O_{1.90}$ in the fluorite structure with 5% oxide ion vacancy. Pd(3d) peaks in the XPS in 1 at. % Pd/CeO_2 are shifted by 3 eV indicating that Pd is in a highly ionic +2 state. EXAFS studies show the average coordination number of 3 around Pd^{2+} ion in the first shell of 1 at. % Pd/CeO_2 at a distance of 2.02 Å, instead of 4 as in PdO. The second shell at 2.72 Å is due to Pd−Pd correlation which is larger than 2.69 Å in PdO. The third shell at 3.31 Å having 7 coordination is absent either in Pd metal or PdO, which can be attributed to $-Pd^{2+}-Ce^{4+}-$ correlation. Thus, 1 at. % Pd/CeO_2 forms the $Ce_{1-x}Pd_xO_{2-\delta}$ type of solid solution having $-Pd^{2+}-O^{2-}-Ce^{4+}-$ kinds of linkages.

Introduction

The structure, active species, and properties of dispersed metal catalyst materials have been of great interest in heterogeneous catalysis for many years. The catalytic activity of the dispersed metals on the supports is influenced by many factors such as relative amount of metals present, extent of dispersion, chemical nature of the support, and strength of interaction between support and the metal.[1] Metals can be dispersed by coprecipitation, deposition, impregnation, ion exchange, sol−gel, and incipient wetness methods.[1,2] Combustion technique has recently been found to be unique in dispersing the metals in the ionic as well as the metallic state on CeO_2 and Al_2O_3 supports.[3−5]

Recently, much attention has been focused on CeO_2-based materials for their applications in automotive exhausts, oxygen storage capacity, and stabilization of dispersed metals.[6−13] Several investigators have reported the noble metal-ceria interaction and its effects on catalytic activities. Like other noble metals, Pd-based catalysts are active for NO reduction and CO and hydrocarbon oxidation reactions.[14−22] Primavera et al. have shown the beneficial catalytic effect of the presence

* Corresponding author. E-mail: mshegde@sscu.iisc.ernet.in, partho@sscu.iisc.ernet.in.
[†] Goa University.
[‡] Indian Institute of Science.
[§] Osaka University.
[¶] Okayama University.
[||] Inter University Consortium.

(1) Augustine, R. L. In *Heterogeneous Catalysis for the Synthetic Chemist*; Marcel Dekker: New York, 1996; p 153.
(2) Janssen, F. J. In *Handbook of Heterogeneous Catalysis*; Ertl, G., Knözinger, H., Weitkamp, J., Eds.; VCH: Weinheim, 1997; Vol. 1, p 191.
(3) Bera, P.; Aruna, S. T.; Patil, K. C.; Hegde, M. S. *J. Catal.* **1999**, *186*, 36.
(4) Bera, P.; Patil, K. C.; Jayaram, V.; Hegde, M. S.; Subbanna, G. N. *J. Mater. Chem.* **1999**, *9*, 1801.
(5) Bera, P.; Patil, K. C.; Jayaram, V.; Subbanna, G. N.; Hegde, M. S. *J. Catal.* **2000**, *196*, 293.
(6) Miki, T.; Ogawa, T.; Haneda, M.; Kakuta, N.; Ueno, A.; Tateishi, S.; Matsuura, S.; Sato, M. *J. Phys. Chem.* **1990**, *94*, 6464.
(7) Terribile, D.; Trovarelli, A.; de Leitenburg, C.; Dolcetti, G. *Chem. Mater.* **1997**, *9*, 2676.
(8) Martínez-Arias, A.; Coronado, J. M.; Cataluña, R.; Conesa, J. C.; Soria, J. *J. Phys. Chem. B* **1998**, *102*, 4357.
(9) Harrison, P. G.; Ball, I. K.; Azelee, W.; Daniell, W.; Goldfarb, D. *Chem. Mater.* **2000**, *12*, 3715.
(10) Martínez-Arias, A. Fernández-García, M.; Salamanca, L. N.; Valenzuela, R. X.; Conesa, J. C.; Soria, J. *J. Phys. Chem. B* **2000**, *104*, 4038.
(11) Luo, M.; Chen, J.; Chen, L.; Lu, J.; Feng, Z.; Li, C. *Chem. Mater.* **2001**, *13*, 197.
(12) Kulyova, S. P.; Lunina, E. V.; Lunin, V. V.; Kostyuk, B. G.; Muravyova, G. P.; Kharlanov, A. N.; Zhilinskaya, E. A.; Aboukaïs, A. *Chem. Mater.* **2001**, *13*, 1491.
(13) Harrison, P. G.; Daniell, W. *Chem. Mater.* **2001**, *13*, 1708.
(14) Graham, G. W.; Logan, A. D.; Shelef, M. *J. Phys. Chem.* **1993**, *97*, 5445.
(15) Yao, Y.-F. Y. *J. Catal.* **1984**, *87*, 152.
(16) Ribeiro, F. H.; Chow, M.; Betta, R. A. D. *J. Catal.* **1994**, *146*, 537.

10.1021/cm0103895 CCC: $22.00
Published on Web 04/24/2002

of Pd in the lattice of ceria-based catalysts for methane combustion.[23] Fernández-García et al.[24] have studied the influence of ceria on Pd activity for CO + O_2 reaction. In all the studies, Pd is believed to be dispersed either as fine metal particles or as surface-oxidized Pd metal. Our recent study[5] showed that Pd^{2+} ions are dispersed on CeO_2, and catalytic activity of ionically dispersed Pd on CeO_2 is much higher than dispersed Pd metal particles on Al_2O_3. Substitution of Pd^{2+} ions for Ce^{4+} in nano CeO_2 particles can lead to the highest possible dispersion for a given loading of Pd and higher chemical and structural stability of Pd^{2+} ions because of the oxygen bonded to Ce^{4+} ions in the CeO_2 matrix.

In the past few years, extended X-ray absorption fine structure (EXAFS) analysis has been used extensively for probing the local structure and identification of the active species of Pd supported on Al_2O_3, niobia, La−Al_2O_3, zeolite, and carbon materials.[25−31] It provides information on the local environment of Pd such as coordination number and the kind of neighboring atoms and their distances with respect to a particular atom. Recently, Matsumura et al.[32,33] investigated the structural change of palladium particles supported on CeO_2 by EXAFS and concluded that during reaction the palladium particles in the catalysts are oxidized because of the formation of Pd−O−Ce bonding. In general, 0.5−2 at. % of noble metals dispersed on CeO_2 are used as the catalyst; therefore, the structure of 1 at. % Pd/CeO_2 is important for understanding its catalytic properties. To glean an insight into the structure and chemical properties of the Pd/CeO_2 catalyst, we have investigated the electronic structure, local environment, and possible substitution of Pd^{2+} ions for Ce^{4+} in CeO_2 by X-ray diffraction (XRD), X-ray photoelectron spectroscopy (XPS), and EXAFS techniques.

Experimental Section

Synthesis. The combustion mixture for the preparation of 1 at. % Pd/CeO_2 materials contained $(NH_4)_2Ce(NO_3)_6$, $PdCl_2$ and $C_2H_6N_4O_2$ (oxalyldihydrazide) in the mole ratio 0.99:0.01:2.33. In a typical preparation, 10 g of $(NH_4)_2Ce(NO_3)_6$ (Fluka, 99.9%), 0.033 g of $PdCl_2$ (Glaxo India Ltd., 99%), and 5.175 g of oxalyldihydrazide were dissolved in the minimum volume of water in a borosilicate dish with 130-cm^3 capacity. The dish containing the redox mixture was introduced into a muffle furnace maintained at 350 °C. Initially the solution boiled with frothing and foaming and ignited to burn with a flame (∼1000 °C) yielding a voluminous solid product within 5 min. Even though 1 at. % Pd/CeO_2 was used for all the catalytic reactions, 5 and 10% Pd/CeO_2 materials were also prepared to examine the nature of Pd in CeO_2. The color of 1 at. % Pd/CeO_2 is light gray; 5 and 10 at. % Pd/CeO_2 samples are deep gray.

We also prepared 1 at. % Pd dispersed on CeO_2 by reducing $PdCl_2$ solution over combustion-synthesized CeO_2 by hydrazine hydrate. The 1 at. % Pd dispersed CeO_2 was thoroughly washed with distilled water, dried at 100 °C, and heated at 200 °C for 12 h. The color of the sample is ash. This catalyst is called 1 at. % Pd/CeO_2 (dispersed) throughout.

Catalytic Test. The catalytic reactions were conducted in a homemade temperature-programmed reaction system equipped with a quadrupole mass spectrometer QXK300 (VG Scientific Ltd., England) for product analysis with a packed-bed tubular reactor.[5] Typically 50 mg of each of the materials were mixed with 150 mg SiO_2 diluent, and it was loaded in a quartz tube reactor of 20-cm length and 6-mm diameter. The reactor can be heated from 30 to 750 °C at a rate of 15 °C min^{-1}, and the sample temperature was measured by a fine chromel−alumel thermocouple immersed in the catalyst. The quartz tube was evacuated to 10^{-6} Torr. The gaseous products were sampled through a fine control-leak valve to an ultrahigh vacuum (UHV) system housing the quadrupole mass spectrometer at 10^{-9} Torr. The gases were passed over the catalyst at a flow rate of 25 μmol s^{-1}. Accordingly, space velocity was 5.0×10^{-4} mol g^{-1} s^{-1}. The dynamic pressure of gases was 10 Torr in the reaction system in all of the experiments. All the masses were scanned in every 10 s. At the end of the reaction, the intensity of each mass as a function of temperature (thermogram) was generated. NO, CO, and O_2 gases were obtained from Bhoruka Gases Ltd., Bangalore. Their purities were better than 99% as analyzed by the quadrupole mass spectrometer.

Characterization. XRD data of Pd/CeO_2 catalyst materials for Rietveld refinement were collected on a Rigaku-2000 diffractometer with a rotating anode with $CuK\alpha_1$ radiation (1.540 59 Å) having a graphite-crystal monochromator. Data were recorded at a scan rate of 1° min^{-1} with 0.02° step size in the 2θ range 20 to 100°, and the structure was refined using the FullProf-98 program. The number of parameters refined simultaneously was 19.

XPS of these materials were recorded in an ESCA-3 Mark II spectrometer (VG Scientific Ltd., England) with AlKα radiation (1486.6 eV). Binding energies were calculated with respect to C(1s) at 285 eV. Binding energies were measured with a precision of 0.2 eV. For XPS analysis, the powder samples were made into pellets of 8-mm diameter and placed in an UHV chamber at 10^{-9} Torr housing the analyzer. Before the sample was mounted in the analyzing chamber, it was kept in the preparation chamber at 10^{-9} Torr for 5 h to desorb any volatile species present on the sample.

Pd K-edge EXAFS spectra in catalyst and reference samples were recorded at room temperature in the transmission mode by using synchrotron radiation with a Si (111) double-crystal monochromator at BL01B1 beamline in Japan Synchrotron Radiation Research Institute (SPring-8), Japan. The monochromator was detuned slightly to reduce the amount of higher harmonics in the beam. The slit width of the monochromator exit was 1 mm vertical and 5 mm horizontal to the optimal resolution. During the measurement the synchrotron was operated at an energy of 8 GeV and a current between 80 and 100 mA. The spectra were scanned in the range 24 200 to 25 600 eV because Pd K-edge energy is 24 348 eV in EXAFS. The photon energy was calibrated for each scan with the first inflection point of Pd K-edge in Pd metal foil. Both the incident (I_o) and transmitted (I) synchrotron beam intensities were measured simultaneously by using an ionization chamber filled with 100% Ar gas and a mixture of 50% Ar and 50% Kr gases, respectively. The absorbers were made by pressing the fine-powder samples into pellets of 10-mm diameter with boron nitride. To avoid the sample thickness effect, the edge step ($\Delta\mu_o x$) was restricted to a value ≤1 by adjusting the thickness

(17) Rainer, D. R.; Koranne, M.; Vesecky, S. M.; Goodman, D. W. *J. Phys. Chem. B* **1997**, *101*, 10769.
(18) Su, S. C.; Carstens, J. N.; Bell, A. T. *J. Catal.* **1998**, *176*, 125.
(19) Cordatos, H.; Gorte, R. J. *J. Catal.* **1996**, *159*, 112.
(20) Almusaiteer, K.; Chuang, S. C. *J. Catal.* **1998**, *180*, 161.
(21) Landry, S. M.; Betta, R. A. D.; Lü, J. P.; Boudart, M. *J. Phys. Chem.* **1990**, *94*, 1203.
(22) Choi, K. I.; Vannice, M. A. *J. Catal.* **1991**, *131*, 1.
(23) Primavera, A.; Trovarelli, A.; de Leitenburg, C.; Dolcetti, G.; Llorca, J. *Stud. Surf. Sci. Catal.* **1998**, *119*, 87.
(24) Fernández-García, M.; Martínez-Arias, A.; Salamanca, L. N.; Coronado, J. M.; Anderson, J. A.; Conesa, J. C.; Soria, J. *J. Catal.* **1999**, *187*, 474.
(25) Lesage-Rosenberg, E.; Vlaic, G.; Dexpert, H.; Lagarde, P.; Freund, E. *Appl. Catal.* **1986**, *22*, 211.
(26) Renouprez, A. J.; Trillot, J. F.; Moraweck, B.; Massardier, J.; Bergeret, G. *J. Catal.* **1998**, *179*, 390.
(27) Noronha, F. B.; Schmal, M.; Moraweck, B.; Delichère, P.; Brun, M.; Villain, F.; Fréty, R. *J. Phys. Chem. B* **2000**, *104*, 5478.
(28) Cho, S. J.; Kang, S. K. *J. Phys. Chem. B* **2000**, *104*, 8124.
(29) Holles, J. H.; Davis, R. J. *J. Phys. Chem. B* **2000**, *104*, 9653.
(30) Okamura, K.; Niwa, M. *J. Phys. Chem. B* **2000**, *104*, 9670.
(31) Park, E. D.; Choi, S. H.; Lee, J. S. *J. Catal.* **2000**, *194*, 33.
(32) Shen, W.-J.; Ichihashi, Y.; Okamura, M.; Matsumura, Y. *Catal. Lett.* **2000**, *64*, 23.
(33) Matsumura, Y.; Shen, W.-J.; Ichihashi, Y.; Ando, H. *Catal. Lett.* **2000**, *68*, 181.

of the absorber pellet where $\Delta\mu_o$ is the edge step in the absorption coefficient and x is the sample thickness.[34]

EXAFS Data Analysis. EXAFS data were analyzed by using the UWXAFS program,[35] which uses the criteria of good background removal, optimization of low R portion of the EXAFS data, and Fourier transform to R space. In principle, the EXAFS function $\chi(k)$ is defined by the relation

$$\chi(k) = [\mu(k) - \mu_o(k)]/\mu_o(k) \quad (1)$$

where μ and μ_o are the characteristic atomic absorption coefficients of the atom in the material of interest and in the isolated state, respectively, both of which are functions of k, which is wave vector of photoelectron ejected as a consequence of X-ray absorption. In practice, EXAFS function $\chi(k)$ is normalized by a constant, the edge-step $\Delta\mu_o$, rather than by a function μ_o. Thus, the normalized EXAFS function $\chi(k)$ is given by

$$\chi(k) = [\mu(k) - \mu_o(k)]/\Delta\mu_o \quad (2)$$

Because the EXAFS function is a superposition of an unknown number of coordination shells, the Fourier transform (FT) technique was used to obtain information about the individual shells. The FT of EXAFS function $\chi(k)$ to R space with k^n weighting factor and Hanning window function (Dk1 and Dk2 = 0.1) was performed in 3−12 Å^{-1} yielding a function $\Phi(R)$. The function $\Phi(R)$, where R is the distance from the absorber atom, is called a radial structure function (RSF) or radial distribution function (RDF). As $\chi(k)$ decreases with increasing k the factor k^n is used to weight the data according to the value of k. In practice, transform with $n = 1$, 2, 3 were used routinely depending on amplitude variation and signal-to-noise ratio of the measured signal. The value of amplitude reduction factor (S_o^2) was deduced from Pd K-edge EXAFS of PdO with known crystal structure data.[36] The theoretical calculations of backscattering amplitude and phase-shift functions were obtained by using the FEFF (6.01) program.[37] The experimental EXAFS data were fitted with the theoretical EXAFS function by using the FEFFIT (2.5 d) program.[38] E_o is one of the fitting parameters in the FEFFIT program. The final values of E_o obtained were 24 348 and 24 353 eV for Pd metal and PdO, respectively. For 5 at. % Pd/CeO_2, the value of E_o obtained was 24 353 eV, and for 1 at. % Pd/CeO_2, the value obtained was 24 354 eV. The goodness of fit was judged by means of χ^2, reduced χ^2, and R factor discussed elsewhere.[39,40] The values of the R factor obtained were 0.01, 0.04, 0.02, and 0.02 for Pd metal, PdO, 5 at. % Pd/CeO_2, and 1 at. % Pd/CeO_2, respectively. From this analysis structural parameters such as coordination numbers (N), bond distance (R), and Debye−Waller factor (σ) were calculated.

Results

Catalytic Studies. CO oxidation by O_2 was performed over polyol-synthesized Pd metal particles (~5−6 nm size), PdO, 1 at. % Pd/CeO_2, and 1 at. % Pd/CeO_2 (dispersed). In Figure 1, % CO conversion over all these materials is shown. Complete CO oxidation occurs below 175 °C over 1 at. % Pd/CeO_2, whereas the same reaction under identical conditions requires 250, 350, and 275 °C over PdO, Pd metal particles, and 1 at. % Pd/CeO_2 (dispersed), respectively. Complete CO oxidation occurs below 175 °C over 5 at. % Pd/CeO_2 prepared by the combustion method.

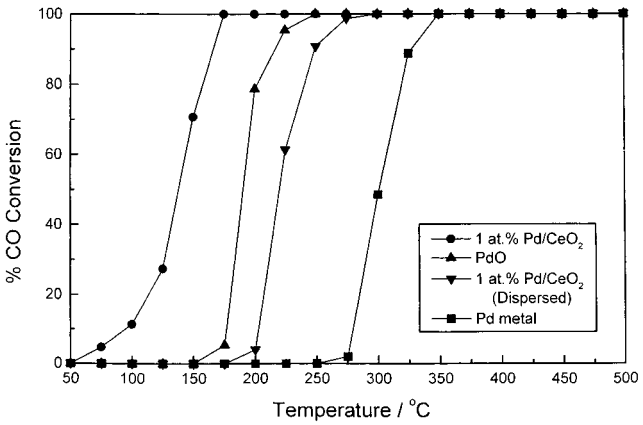

Figure 1. Percent CO conversion over 1 at. % Pd/CeO_2, PdO, 1 at. % Pd/CeO_2 (dispersed), and Pd metal for CO + O_2 reaction.

The reaction temperatures over these catalyst materials follow the same trend for the NO + CO reaction. Increase in CO_2/N_2O (m/z = 44) concentration with simultaneous decrease in NO (m/z = 30) is taken as the measure of NO conversion. If N_2O is formed during the reaction because of partial reduction of NO, it is not possible to distinguish between N_2O and CO_2 because the mass number of N_2O is the same as that of CO_2 (m/z = 44). Temperature-programmed reaction profiles of the NO + CO reaction as a function of temperature are given in Figure 2a. Catalytic reduction of NO by NH_3 over the same 1 at. % Pd/CeO_2 catalyst shows trace amounts of N_2O formation along with N_2 and H_2O in the temperature range of 250 to 300 °C and at higher temperature it decomposes and N_2 and H_2O are only products. Therefore, possibility of formation of N_2O to a some extent cannot be ruled out during the NO + CO reaction. Nonetheless, NO conversion at a lower temperature over 1 at. % Pd/CeO_2 prepared by the combustion method compared with other catalysts is clear from Figure 2b. Therefore, it is essential to understand the structure of 1 at. % Pd/CeO_2 catalyst synthesized by the solution combustion method.

XRD Studies. Observed, calculated, and difference XRD patterns of 1 and 5 at. % Pd/CeO_2 are shown in Figure 3. The diffraction lines are indexed for fluorite structure. The diffraction lines corresponding to Pd or PdO are not observed in the XRD pattern of 1 at. % Pd/CeO_2 (Figure 3a). Even a slow scan in Pd (111) region ($2\theta \approx 40 \pm 5°$) does not show any indication of Pd metal peaks. However, 5 at. % Pd/CeO_2 does show Pd metal peaks (Figure 3b). Rietveld refinements of pure CeO_2, 1 at. % Pd/CeO_2, and 5 at. % Pd/CeO_2 are performed by varying overall scale factor, background parameters, unit cell, shape and isotropic thermal parameters, along with the oxygen occupancy. In pure CeO_2, the structure could be refined to R_{Bragg} factor of 0.91%. Oxygen deficiency is found to be of the order of 3.5%. Recent studies of lattice defects in CeO_2 by Mamontov et al.[41] have also shown oxygen vacancies to the extent of 4% in the nano crystalline CeO_2. They have suggested that,

(34) Stern, E. A.; Kim, K. *Phys. Rev. B* **1981**, *23*, 3781.
(35) Newville, M.; Livins, P.; Yacobi, Y.; Rehr, J. J.; Stern, E. A. *Phys. Rev. B* **1993**, *47*, 14126.
(36) Pearson, W. P. In *Handbook of Lattice Spacings and Structures of Metals and Alloys*; Pergamon: New York, 1958.
(37) Zabinski, S. I.; Rehr, J. J.; Ankudinov, A.; Albers, R. C.; Eller, M. J. *Phys. Rev. B*, **1995**, *52*, 2996.
(38) Stern, E. A.; Newville, M.; Ravel, B. D.; Yacoby, Y.; Haskel, D. *Physica B* **1995**, *208 & 209*, 117.
(39) Press, W. H.; Teulosky, S. A.; Vetterling, W. T.; Flannery, B. P. In *Numerical Recipies*; Cambridge University Press: New York, 1992.
(40) Bevington, P. R. In *Data Reduction and Error Analysis for Physical Sciences*; McGraw-Hill: New York, 1969.

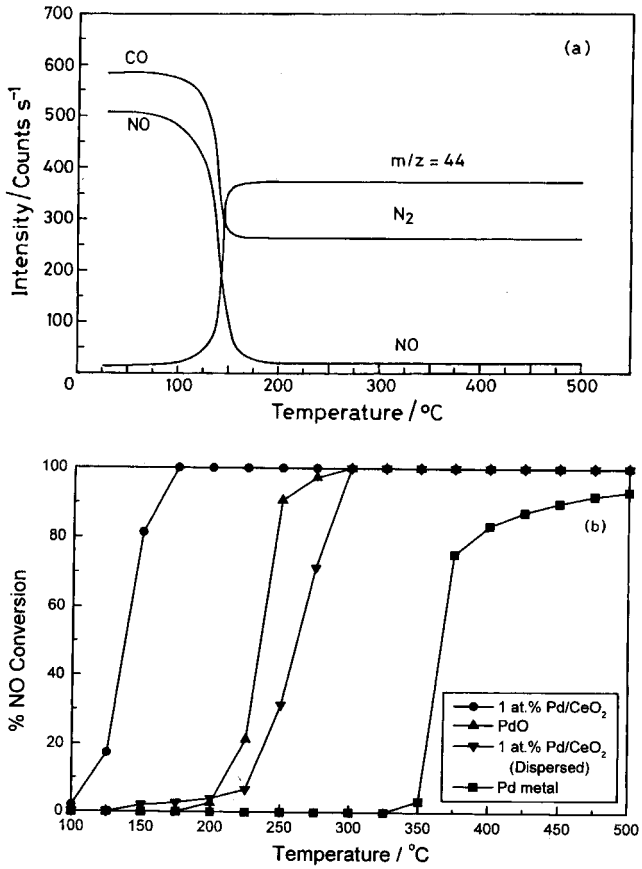

Figure 2. (a) Temperature-programmed reaction profiles of NO + CO reaction over 1 at. % Pd/CeO_2, (b) percent NO conversion over 1 at. % Pd/CeO_2, PdO, 1 at. % Pd/CeO_2 (dispersed), and Pd metal for NO + CO reaction.

in addition to oxygen vacancies in the tetrahedral site, Frenkel type of oxygen in the interstitial octahedral site is stabilized in ceria-zirconia solid solution. In 1 at. % Pd/CeO_2, the structure could be refined to R_{Bragg} factor of 0.89%, and the oxygen deficiency is 5%. The 'a' parameter also decreases from 5.4113(2) Å in pure CeO_2 to 5.4107(2) Å in 1 at. % Pd/CeO_2. Accordingly, composition obtained from the fitting is $Ce_{0.99}Pd_{0.01}O_{1.90}$. XRD data of 5 at. % Pd/CeO_2 could be refined for the composition of $Ce_{0.97}Pd_{0.03}O_{1.87}$ and Pd metal phase. Here, the oxygen vacancy is found to be 6.5%. Lattice parameter 'a' decreases to 5.4101 (2) Å in 5 at. % Pd/CeO_2. Intensity of Pd(111) peak in 5 at. % Pd/CeO_2 and 2 at. % Pd + CeO_2 mixture are about same. XRD pattern of 10 at. % Pd/CeO_2 shows an increased Pd(111) peak intensity. However, peaks due to PdO could not be detected. Here also the pattern could be refined to $Ce_{0.97}Pd_{0.03}O_{1.87}$ and Pd metal phase. The lattice parameter is 5.4101(2) Å indicating that there is a limit of Pd substitution in CeO_2 matrix. A systematic increase in oxygen deficiency from 3% in pure CeO_2 to about 5% in 1 at. % Pd/CeO_2 is an indication of Pd^{2+} ion incorporation to Ce^{4+} sites. Even in 5 and 10 at. % Pd/CeO_2, PdO phase could not be detected but Pd metal peak is observed. Thus, Rietveld analyses suggest that a maximum 3 at. % Pd^{2+} ion can be substituted in Ce^{4+} sites. It is also possible that Pd^{2+} ions can be incorporated in

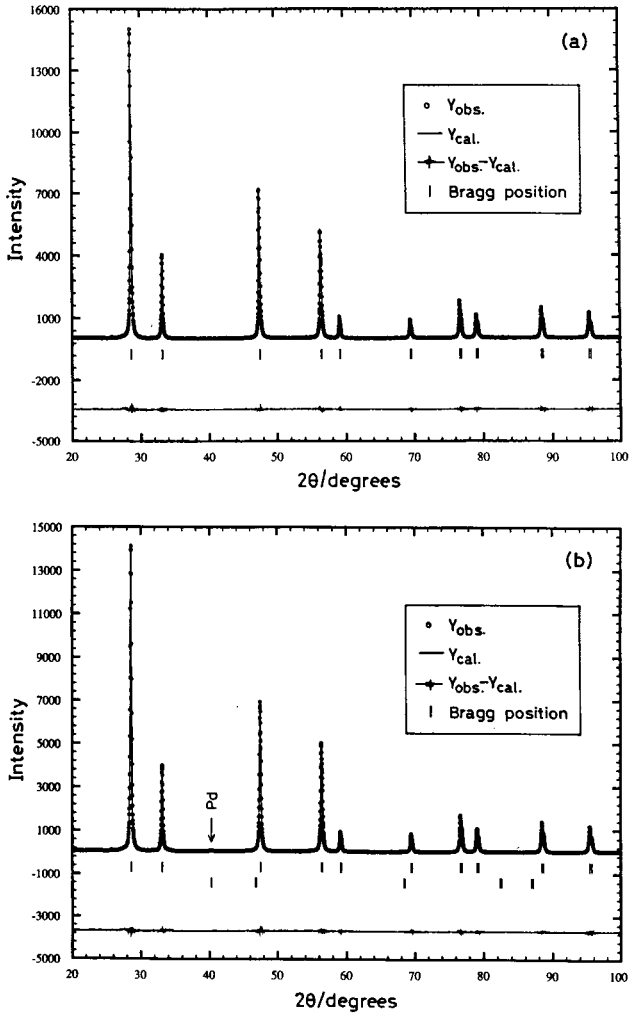

Figure 3. Observed, calculated, and difference XRD patterns of (a) 1 at. % Pd/CeO_2, and (b) 5 at. % Pd/CeO_2.

the interstitial sites. However, from Rietveld refinement it has not been possible to find if the oxygen defects are present around Pd^{2+} ions or distributed in the whole matrix. Diffraction lines due to Pd metal or PdO phase are not observed even with slow scan in the XRD pattern of 1 at. % Pd/CeO_2 (dispersed).

XPS Studies. XPS of Pd(3d) core level region of 1 and 5 at. % Pd/CeO_2 and 1 at. % Pd/CeO_2 (dispersed) are given in Figure 4. Pd($3d_{5/2,3/2}$) peaks were resolved into sets of spin−orbit doublets. Accordingly, Pd($3d_{5/2,3/2}$) peaks are observed at 338.0 and 342.8 eV in 1 at. % Pd/CeO_2 (Figure 4a). Recent XPS studies[42,43] of Pd metal and PdO show that binding energies of Pd($3d_{5/2}$) in Pd metal and PdO are at 335.4 and 336.8 eV, respectively. We have confirmed these values for Pd metal and PdO. Thus, Pd core levels in 1 at. % Pd/CeO_2 catalyst are shifted by 2.6 eV with respect to Pd metal, whereas Pd(3d) shift is 1.2 eV in comparison with PdO. Binding energies of Pd(3d) peaks in 1 at. % Pd/CeO_2 agree well with those of Pd^{2+} in $PdCl_2$ and $Pd(NO_3)_2$ clearly indicating that Pd^{2+} ions are much more ionic in CeO_2 matrix than PdO. Absence of PdO peaks in the diffrac-

(41) Mamontov, E.; Egami, T.; Brezny, R.; Koranne, K.; Tyagi, S. *J. Phys. Chem. B* **2000**, *104*, 11110.

(42) Pillo, T.; Zimmermann, R.; Steiner, P.; Hüfner, S. *J. Phys. Condens. Matter* **1997**, *9*, 3987.

(43) Burn, M.; Berthet, A.; Bertolini, J. C. *J. Electron Spectrosc. Relat. Phenom.* **1999**, *104*, 55.

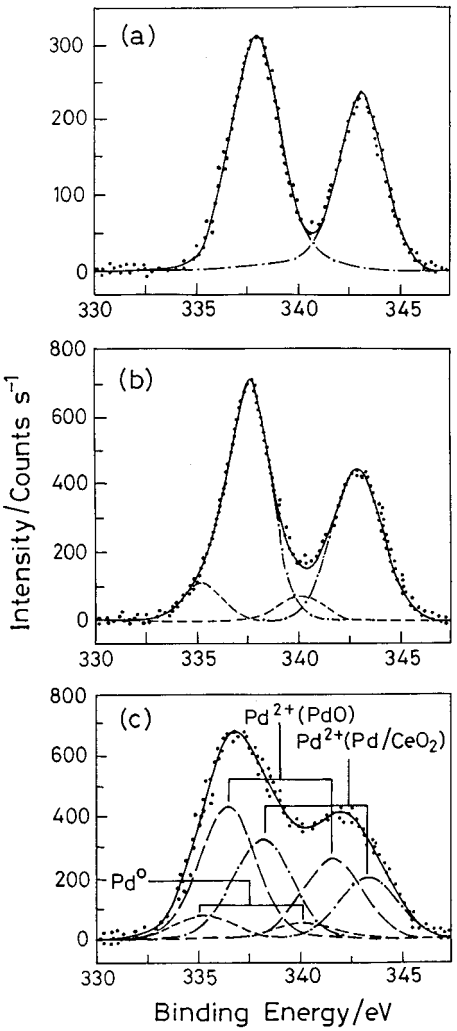

Figure 4. XPS of Pd(3d) core level region of (a) 1 at. % Pd/CeO_2, (b) 5 at. % Pd/CeO_2, and (c) 1 at. % Pd/CeO_2 (dispersed).

tion patterns as seen from XRD studies correlates with the XPS results. However, a careful XPS study of Pd(3d) region in 5 at. % Pd/CeO_2 shows the corresponding peaks of Pd^{2+} ion as in 1 at. %Pd/CeO_2 along with Pd metal (Figure 4b). Pd($3d_{5/2,\ 3/2}$) peaks at 335.2 and 340.2 eV can be assigned to Pd^o, and 337.9 and 343.0 eV peaks can be attributed to Pd^{2+} as in 1 at. % Pd/CeO_2. Relative intensity of Pd($3d_{5/2}$) peak of Pd^o to Pd^{2+} is 0.15 indicating that, even in 5 at. % Pd/CeO_2, Pd is present mostly in the Pd^{2+} state. The Pd(3d) region of 1 at. % Pd/CeO_2 (dispersed) is shown in Figure 4c. The spectrum shows more than one Pd species compared with 1 at. % Pd/CeO_2 synthesized by the combustion method. The spectrum could be resolved into three sets of spin−orbit doublets. Accordingly, Pd($3d_{5/2,\ 3/2}$) peaks at 335.3, 340.2; 336.6, 341.6, and 338.2, 343.3 eV could be attributed to Pd^o, PdO, and Pd in CeO_2 like 1 at. % Pd/CeO_2. Intensity of Pd($3d_{5/2,\ 3/2}$) peaks at 336.6 and 341.6 eV due to PdO is much higher than Pd^o. Further, corresponding peaks of Pd^{2+} attributable to Pd in CeO_2 matrix at 338.2 and 343.3 eV is also present in the sample. Thus, 1 at. % Pd/CeO_2 (dispersed) contains mostly PdO species over CeO_2. Therefore, XPS of 1 at. % Pd/CeO_2 by the combustion method clearly indicates that Pd is present in a highly ionic Pd^{2+} state. Ce(3d)

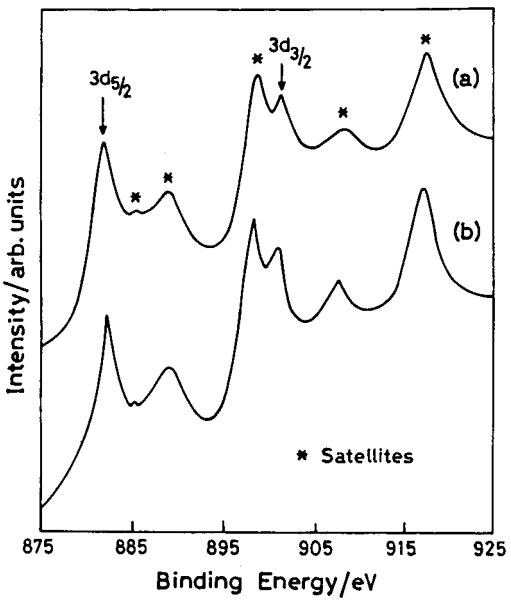

Figure 5. XPS of Ce(3d) core level region of (a) 1 at. % Pd/CeO_2, and (b) 5 at. % Pd/CeO_2.

peaks observed in 1 and 5 at. % Pd/CeO_2 are shown in Figure 5. The spectra with satellite features (marked in the figure) correspond to CeO_2 with Ce in +4 oxidation state. There may be a trace component of reduced CeO_2 in the spectrum due to Ce^{3+} as obtained in UHV (10^{-9} Torr) conditions.[44] The surface concentration of metal ions in Pd/CeO_2 catalysts have been calculated by the relation

$$\frac{X_{Pd}}{X_{Ce}} = \frac{I_{Pd}}{I_{Ce}} \frac{\sigma_{Ce}\lambda_{Ce}D_E(Ce)}{\sigma_{Pd}\lambda_{Pd}D_E(Pd)} \qquad (3)$$

where X, I, σ, λ, and D_E are surface concentration, intensity, photoionization cross-section, mean escape depth, and geometric factors, respectively. Integrated intensities of Pd(3d) and Ce(3d) peaks have been taken into account to estimate the concentration. Photoionization cross-section and mean escape depths have been obtained from the literature.[45,46] Surface concentrations of Pd^{2+} ions are 5 and 18% in 1 and 5 at. % Pd/CeO_2, respectively.

EXAFS Studies. In Figure 6, Pd K-edge XANES spectra of 1 at. % Pd/CeO_2, 5 at. % Pd/CeO_2, 10 at. % Pd/CeO_2, PdO, and Pd metal are presented. The Pd K-edge in Pd metal shows two peaks characteristic of transition metals. However, no splitting of the edge is observed. The second absorption peak is stronger than the first, because the absorption cross-section in the K-edge region of transition metals is strongly influenced by d−s,p hybridization caused by unoccupied d bands. Thus, in the systems where the d−s, p hybridization is strong, the p-like density of states is strongly enhanced and the absorption can be increased like the second absorption peak in the XANES spectrum of the Pd foil. The XANES spectra of PdO in the figure show the

(44) Laachir, A.; Perrichon, V.; Badri, A.; Lamotte, J.; Catherine, E,; Lavalley, J. C.; Fallah, J. E.; Hilaire, L.; le Normand, F.; Quéméré, E.; Sauvion, G. N.; Touret, O. *J. Chem. Soc., Faraday Trans.* **1991**, *87*, 1601.
(45) Scofield, J. H. *J. Electron Spectrosc. Relat. Phenom.* **1976**, *8*, 129.
(46) Penn, D. R. *J. Electron Spectrosc. Relat. Phenom.* **1976**, *9*, 29.

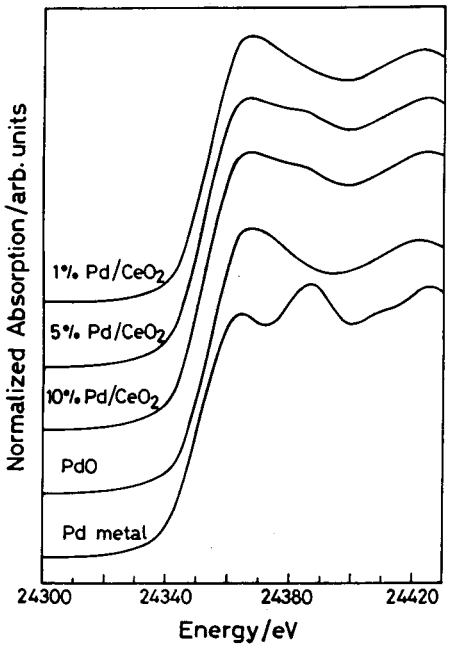

Figure 6. Normalized XANES spectra of (a) Pd metal, (b) PdO, (c) 10 at. % Pd/CeO_2, (d) 5 at. % Pd/CeO_2, and (e) 1 at. % Pd/CeO_2.

strong absorption at the Pd K-edge, because the d−p hybridization of Pd^{2+} significantly increases the absorption cross-section, compared with that of Pd foil.

The XANES feature is very sensitive to long-range order up to 10 nm because of the large mean free path of the photoelectron in the energy range of 1−100 eV above the absorption edge.[47] The reference Pd and PdO spectra thus have characteristic XANES features that are sensitive to the change in physicochemical environment of the absorbing Pd atom, such as change of oxidation state. Figure 6 shows that the XANES spectra of 10 and 5 at. % Pd/CeO_2 are distinctly different from 1 at. % Pd/CeO_2. With some subtle differences, 1 at. % Pd/CeO_2 spectrum is similar to that of PdO. The positions of first minimum and next maximum after the edge in 1% Pd/CeO_2 are at high energies as compared with those in PdO. On the other hand, an additional weak peak at ~20 eV from the main absorption peak is seen in 5 and 10 at. % Pd/CeO_2. The energy of this peak matches with the second strong absorption peak in Pd metal. This seems to indicate that the 5 and 10 at. % Pd/CeO_2 samples contain two species of Pd, one in a metal-like state and other in a PdO-like state. This agrees well with Rietveld analysis of diffraction data that clearly show the presence of Pd metal, although diffraction lines due to PdO are not seen. Because of this similarity between 5 and 10 at. % samples, we present results only on 5 at. % Pd/CeO_2 along with 1 at. % Pd/CeO_2.

Background subtracted EXAFS functions [$\chi(k)$] of all the materials are shown in Figure 7. The EXAFS of 5 at. % Pd/CeO_2 is distinctly different from that of PdO. The features of 5 at. % Pd/CeO_2 EXAFS spectra can be reproduced by adding the EXAFS of Pd metal and PdO. This clearly indicates the presence of both Pd metal-like and Pd^{2+} species in 5 at. % Pd/CeO_2. In 1 at. % Pd/CeO_2, the EXAFS is similar to that of PdO indicating that Pd is in the Pd^{2+} state.

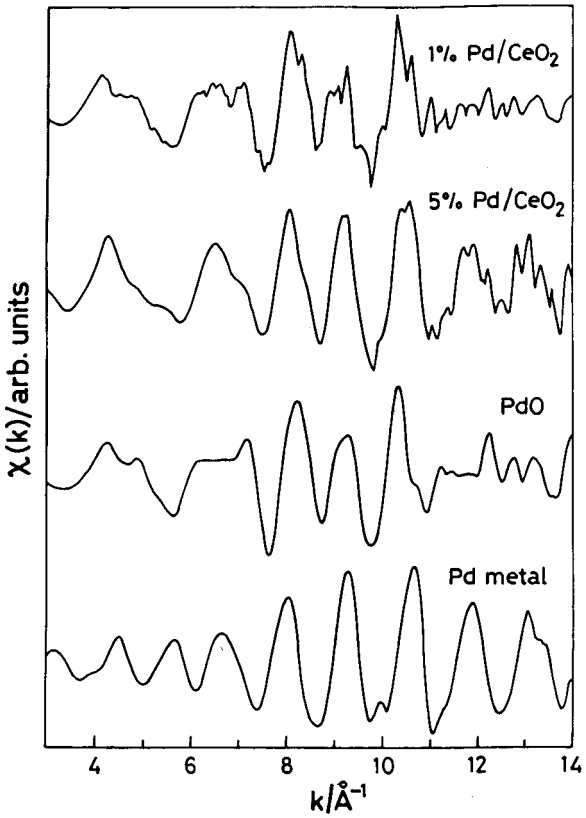

Figure 7. EXAFS function of (a) Pd metal, (b) PdO, (c) 5 at. % Pd/CeO_2, and (d) 1 at. % Pd/CeO_2.

The Fourier transforms of k^3-weighted $\chi(k)$ for all the compounds are presented in Figure 8. These spectra are not corrected for phase shifts so that the observed peaks are shifted to lower R values from the true interatomic distances. The values of bond lengths mentioned in the text and Tables 1 and 2 are, phase corrected, however. In PdO, the first peak at 2.02 Å corresponds to 4 Pd−O bonds, second peak encompasses 2 Pd−Pd bonds at 2.69 Å and 4 Pd−Pd bonds at 3.07 Å, and the third peak has contributions from 8 Pd−O bonds at 3.58 Å and 16 Pd−Pd/O bonds at 3.72 Å. The structural parameters obtained from EXAFS analysis of PdO and Pd metal are summarized in Table 1. The coordination number and bond lengths agree well with Pd metal and PdO crystal structure data.

The catalyst samples show three peaks in the FT spectra as can be seen from Figure 8. PdO has been used as the primary model for fitting of all the catalytic compounds. This is because the XANES features that are signature of the physicochemical environment of the central Pd^{2+} ion are similar to PdO. The first peak around 2.02 Å in catalysts matches with the first peak in PdO, thereby indicating the presence of Pd−O interactions. The second and third peaks in the FT spectrum of 1 at. % Pd/CeO_2 are similar to those in PdO, but they are shifted to higher R values in relation to PdO. The Rietveld analysis of XRD data of 1 at. % Pd/CeO_2 has indicated that Pd^{2+} ions are substituted for Ce^{4+} in CeO_2 structure. Also the binding energy shifts of Pd(3d) peaks for 1 at. % Pd/CeO_2 sample is much higher than those for PdO. Therefore, the local environ-

(47) Grunes, L. A. *Phys. Rev. B* **1983**, *27*, 2711.

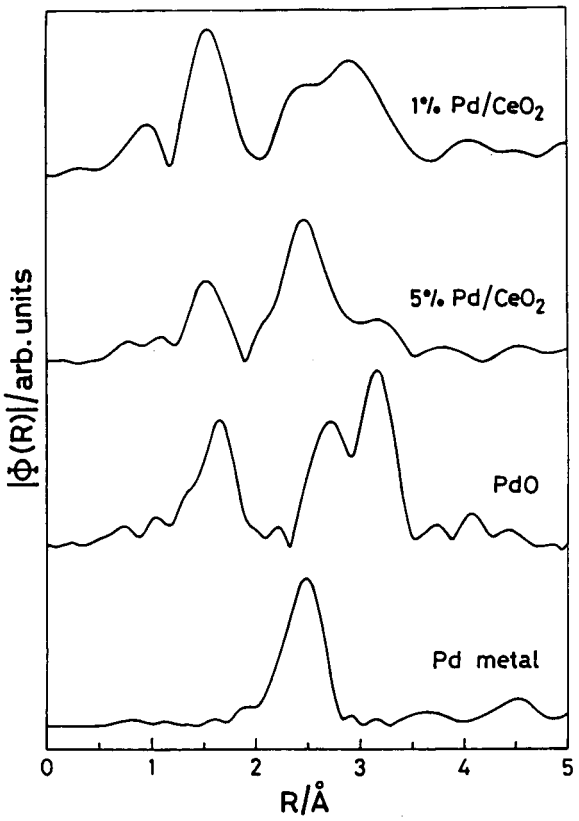

Figure 8. Fourier transforms of (a) Pd metal, (b) PdO, (c) 5 at. % Pd/CeO_2, and (d) 1 at. % Pd/CeO_2.

Table 1. Structural Parameters of Pd Metal Foil and PdO from EXAFS Analysis

samples	shell	*N*	*R* (Å)	σ^2 (Å^{-2})
Pd metal	Pd−Pd	12.0	2.747 ± 0.003	0.006 ± 0.001
		6.0	3.885 ± 0.002	0.009 ± 0.001
		48.0	4.120 ± 0.002	0.008 ± 0.001
		48.0	4.689 ± 0.004	0.050 ± 0.004
		24.0	4.758 ± 0.003	0.008 ± 0.002
PdO	Pd−O	4.0	2.023 ± 0.005	0.002 ± 0.001
	Pd−Pd	2.0	2.694 ± 0.008	0.011 ± 0.003
	Pd−Pd	4.0	3.079 ± 0.009	0.005 ± 0.001
	Pd−O	8.0	3.581 ± 0.002	0.002 ± 0.001
	Pd−O/Pd	16.0	3.721 ± 0.009	0.006 ± 0.001

Table 2. Structural Parameters for Pd/CeO_2 Catalysts Obtained from EXAFS Analysis

catalysts	shell	*N*	*R* (Å)	σ^2 (Å^{-2})
1 at. % Pd/CeO_2	Pd−O	2.7 ± 0.5	2.021 ± 0.003	0.001 ± 0.001
	Pd−Pd	3.2 ± 0.6	2.717 ± 0.006	0.007 ± 0.001
	Pd−Ce	7.3 ± 0.7	3.313 ± 0.004	0.007 ± 0.001
5 at. % Pd/CeO_2	Pd−O	2.7 ± 0.3	2.021 ± 0.004	0.003 ± 0.001
	Pd−Pd	4.0 ± 0.3	2.759 ± 0.001	0.006 ± 0.001
	Pd−Ce	9.5 ± 0.5	3.311 ± 0.004	0.013 ± 0.001

ment of Pd in 1 at. % Pd/CeO_2 is different from the one in PdO phase. In light of Rietveld refinement we considered it worthwhile to use the $Pd-CeO_2$ solid solution model of the type $Ce_{1-x}Pd_xO_{2-\delta}$ for fitting the EXAFS data of 1 at. % Pd/CeO_2 catalyst. For the FEFF calculation, using this solid solution model we have assumed Pd^{2+} as dopant for Ce^{4+} and a lattice parameter of 4.67 Å to account for Pd−O bond length of 2.02 Å. The structural parameters are given in Table 2. The first shell around Pd^{2+} ion with coordination number of 2.7 at 2.02 Å is attributed to Pd−O interaction in 1 at. % Pd/CeO_2 catalyst against 4 in PdO phase. The second shell at 2.72 Å correlates with Pd−Pd interaction and has a coordination number of 3.2. Third correlation at 3.31 Å can be attributed to Pd−Ce interaction. A peak at 3.31 Å is absent in FT spectra of Pd metal or PdO phase.

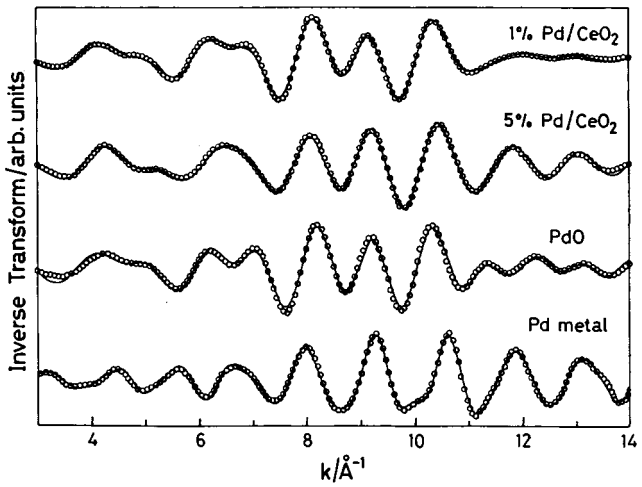

Figure 9. Inverse Fourier transforms of (a) Pd metal, (b) PdO, (c) 5 at. % Pd/CeO_2, and (d) 1 at. % Pd/CeO_2. (Continuous line indicates the fitted curve.)

In the 5 at. % Pd/CeO_2 sample, the intensities of the second and third peaks are different from those of 1 at. % Pd/CeO_2. Furthermore, the second peak, which is much more intense than the third, matches well with the first peak in the FT of Pd metal. Thus, it is evident that the FT spectra of 5 at. % Pd/CeO_2 is difficult to explain only on the basis of $Ce_{1-x}Pd_xO_{2-\delta}$ solid solution model. Rietveld analysis and XANES spectrum of this compound also has indicated the presence of two species of Pd (Pd metal like and Pd^{2+} like). Therefore, we have fitted the FT magnitude using Pd metal and solid solution phase having Pd−O, Pd−Pd, and Pd−Ce interactions. Accordingly, the peak at 2.02 Å corresponds to Pd−O interaction with coordination of 2.7 as in the 1% sample. The second and third peaks can be well fitted by taking Pd−Pd correlation belonging to Pd metal-like phase and to the solid-solution phase at 2.75 Å and Pd−Ce correlation at 3.31 Å. The bond lengths of Pd−Pd in Pd metal and in the solid-solution phase as obtained from our EXAFS studies in the 1 at. % Pd/CeO_2 are very close, and it is difficult to separate them. Further, because the second and third peaks are not well resolved, the values of near neighbors obtained from EXAFS analysis for Pd−Pd and Pd−Ce correlations may not depict actual number of neighbors. The inverse transforms along with fitted curves for catalysts and reference compounds are presented in Figure 9. It is clear from the figure that inverse transform of 1 at. % Pd/CeO_2 is different from PdO phase especially in the *k* range of 11−14 Å^{-1}. The fitted curve assuming the Pd^{2+} ion in the CeO_2 model agrees well with the experimental data.

Discussion

The solution-combustion method produces CeO_2-supported Pd catalysts in a single step. So, in combustion-synthesized Pd/CeO_2, Pd should either be separated into

Pd metal clusters, PdO separated from oxide support, or Pd ion should be incorporated in the CeO_2 lattice. Pure PdO phase could not be detected even in 5 at. % Pd/CeO_2 and Pd metal particles are not observed in 1 at. % Pd/CeO_2. If there is an ionic substitution of Pd^{2+} ions for Ce^{4+} sites in the CeO_2 lattice, oxide ion vacancy should be created to maintain the charge neutrality because of lower valent ionic substitution. Rietveld analysis of XRD data shows the presence of oxide ion vacancy and the structure of Pd/CeO_2 catalysts could be refined to the solid-solution phase of $Ce_{1-x}Pd_xO_{2-\delta}$. Oxide ion vacancy increases from 3.5 to 5% in pure CeO_2 to 1 at. % Pd/CeO_2. XPS studies show that Pd is in a highly ionic state compared with PdO. EXAFS study indicates a lower coordination for Pd^{2+} ion than in PdO indicating an oxide ion vacancy around Pd^{2+} ion. The data analysis shows that Pd is in +2 state and strongly interacts with the CeO_2 support giving rise to Pd−O−Ce interaction. In pure CeO_2, the oxygen ions are tetrahedrally coordinated to Ce^{4+} ions giving a Ce−O−Ce angle of 109.5° and Ce−Ce distance of 3.82 Å. When Pd^{2+} is substituted for Ce^{4+}, a slight modification in the local structure around Pd is expected. The corresponding Pd−O, Pd−Pd, and Pd−Ce correlations obtained from EXAFS studies are 2.02, 2.72, and 3.31 Å. Pd^{2+}−Ce^{4+} correlation at 3.31 Å can only be possible via an oxide ion. Considering the Pd^{2+} is substituted for Ce^{4+} in CeO_2 and with the observed Pd−O−Ce distance of 3.31 Å from radial distribution, Pd−O−Ce angle is calculated to be ∼90°. This is very close to Pd−O−Pd angle in PdO. Ionic radii of Pd^{2+}, O^{2-}, and Ce^{4+} are 0.86, 1.4, and 1.01 Å respectively.[48] Accordingly, Pd^{2+}, O^{2-}, and Ce^{4+} ions with their real sizes in contact at 90° indeed give Pd^{2+}−Ce^{4+} distance of 3.27 Å, which is close to 3.31 Å observed experimentally. X-ray absorption studies of 2−75 nm CeO_2 particles by Nachimuthu et al.[49] show that for smaller particles (2−5 nm) the first coordination number of Ce^{4+} is 6 (O^{2-}) and for the particles of ≥15 nm coordination number is 8. Particle sizes of combustion-synthesized Pd/CeO_2 catalysts are in the range of 15−25 nm and, therefore, Ce^{4+} should have 8 oxide ion coordination following the fluorite structure. In CeO_2, the surface Ce^{4+} ion is coordinated to 4 oxide ions in the first shell. If Pd^{2+} ion is incorporated in to Ce^{4+} site, Pd^{2+} ion should have had oxide ion coordination number of 4. Our EXAFS studies show that coordination number of Pd is about 3. This clearly indicates that oxide ion vacancies are around Pd^{2+} ions on the surface of CeO_2.

From the structural studies of 1 at. % Pd/CeO_2 above, it is evident that Pd^{2+} ions are substituted mostly on ∼30 nm CeO_2 crystallite surface with oxide ion vacancies around Pd^{2+} ions. Because this material contains only Pd^{2+} ions and CO oxidation occurs at much lower temperatures than either Pd metal or PdO or 1 at. % Pd/CeO_2 (dispersed), it can be concluded that Pd^{2+} ions in CeO_2 matrix are the active sites for CO adsorption. Further, NO + CO reaction over Pd/Al_2O_3 and Pd/CeO_2 prepared by sol−gel method[50] occurs at the same temperature as over 1 at. % Pd/CeO_2 (dispersed) reported here. The higher catalytic activity in combustion-synthesized 1 at. % Pd/CeO_2 for CO oxidation in terms of lower reaction temperature can be attributed to the interaction of Pd^{2+} ions with CeO_2 support. Oxide ion vacancy in CeO_2 created by Pd^{2+} ion substitution can now become an oxygen-exchange site. This can be either the oxide ion vacancy in tetrahedral site or an octahedral hole. Based on $Ce_{1-x}Pd_xO_{2-\delta}$ model, CO oxidation mechanism can be written as follows,

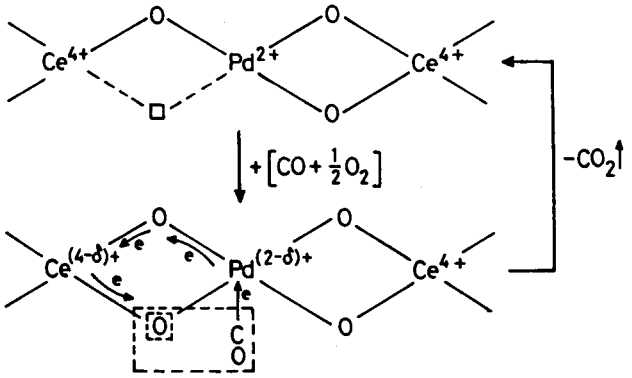

Figure 10. Shematic representation of CO + O_2 reaction over 1 at.% Pd/CeO_2.

$$V_{O^{2-}}^{\bullet\bullet} + {}^1/_2O_2 \rightarrow O_o^x + 2\,h^{\bullet} \quad (4)$$

$$Ce^{4+}-O^{2-}-Pd^{2+} + CO + O_o^x \rightarrow Ce^{4+}-O^{2-}-Pd^{o} + V_{O^{2-}}^{\bullet\bullet} + CO_2 \quad (5)$$

$$Ce^{4+}-O^{2-}-Pd^{o} + h^{\bullet} \rightarrow Ce^{3+}-O^{2-}-Pd^{2+} \quad (6)$$

$$Ce^{3+}-O^{2-}-Pd^{2+} + h^{\bullet} \rightarrow Ce^{4+}-O^{2-}-Pd^{2+} \quad (7)$$

where, $V_{O^{2-}}^{\bullet\bullet}$, O_o^x, and $h^{\bullet}$ are doubly ionized oxide ion vacancy, neutral oxygen occupied in the vacancy and electron hole, respectively. The above reaction sequence is depicted in Figure 10.

Conclusions

The structure and local chemical environment of Pd species in 1 at. % Pd/CeO_2 catalyst have been investigated here. The main findings of our investigation are:

(1) From a comparison of CO + O_2 and NO + CO reactions over Pd nano particles, PdO, 1 at. % Pd/CeO_2, and 1 at. % Pd/CeO_2 (dispersed), it has been shown that Pd^{2+} ions in CeO_2 matrix is the most active catalyst material.

(2) High-resolution XRD shows the absence of the Pd metal or PdO diffraction line in 1 at. % Pd/CeO_2 forming a solid solution, $Ce_{1-x}Pd_xO_{2-\delta}$ ($0 \le x \le 0.03$).

(3) Rietveld refinement confirms the oxide ion vacancy in 1 at. % Pd/CeO_2.

(4) XPS studies show that Pd is in a highly ionic Pd^{2+} state in 1 at. % Pd/CeO_2.

(5) XANES of catalysts show that a Pd^{2+}-like species is present in the catalysts.

(48) Dickinson, S. K., Jr. In *Ionic, Covalent and Metallic Radii of the Chemical Elements*; Airforce Cambridge Research Laboratories: L. G. Hanscom Field, Bedford, MA, 1970.

(49) Nachimuthu, P.; Shih, W.-C.; Liu, R.-S.; Jang, L.-Y.; Chen, J.-M. *J. Solid State Chem.* **2000**, *149*, 408.

(50) Noh, J.; Yang, O.-B.; Kim, D. H.; Woo, S. I. *Catal. Today* **1999**, *53*, 575.

(6) EXAFS analysis proves that Pd^{2+} ions are substituted for Ce^{4+} sites with oxide ion vacancy around Pd^{2+} ion.

(7) The Pd^{2+} ion is stabilized in the Ce^{4+} site leading to a strong $Pd-CeO_2$ interaction in the form of $Ce_{1-x}Pd_xO_{2-\delta}$ solid solution with $-Pd^{2+}-O^{2-}-Ce^{4+}-$ linkages.

Acknowledgment. Indian authors gratefully acknowledge Department of Science and Technology (DST), Government of India, for financial support. Thanks are also due to the authorities of SPring-8, Japan for alloting beamtime at BL01B1 beamline (Proposal 2000A0305-NX-np) and for local hospitality. P. Bera thanks the Council of Scientific and Industrial Research (CSIR), Government of India for the award of a research fellowship. We thank Dr. B. A. Dasannacharya, Director, IUC-DAEF, Indore, for allowing us to use the UWXAFS software for data analysis and for constant encouragement.

CM0103895